Chinese Journal of Natural Medicines

Profiling the chemical differences of diterpenoid alkaloids in different processed products of Aconiti Lateralis Radix Praeparata by UHPLC–LTQ–Orbitrap mass spectrometry combined with untargeted metabolomics and mass spectrometry imaging

Yang Yu, Changliang Yao, Jianqing Zhang, Yong Huang, Shuai Yao, Hua Qu, Tong Zhang, Dean Guo

Citation: Yang Yu, Changliang Yao, Jianqing Zhang, Yong Huang, Shuai Yao, Hua Qu, Tong Zhang, Dean Guo, Profiling the chemical differences of diterpenoid alkaloids in different processed products of Aconiti Lateralis Radix Praeparata by UHPLC–LTQ–Orbitrap mass spectrometry combined with untargeted metabolomics and mass spectrometry imaging, Chinese Journal of Natural Medicines, 2025, 23(8), 1009–1015. doi: 10.1016/S1875–5364(25)60936–8.

View online: https://doi.org/10.1016/S1875–5364(25)60936–8

Wechat

Chinese Journal of Natural Medicines 23 (2025) 1009-1015

Contents lists available at ScienceDirect

Chinese Journal of Natural Medicines

journal homepage: www.cjnmcpu.com/

Original article

Profiling the chemical differences of diterpenoid alkaloids in different processed products of Aconiti Lateralis Radix Praeparata by UHPLC-LTQ-Orbitrap mass spectrometry combined with untargeted metabolomics and mass spectrometry imaging

Yang Yu[a], Changliang Yao[b], Jianqing Zhang[b], Yong Huang[b], Shuai Yao[b], Hua Qu[b], Tong Zhang[a,*], Dean Guo[a,b,*]

[a] *School of Pharmacy, Shanghai University of Traditional Chinese Medicine, Shanghai 201203, China*
[b] *Shanghai Research Center for Modernization of Traditional Chinese Medicine, National Engineering Research Center for TCM Standardization Technology, Shanghai Institute of Materia Medica, Chinese Academy of Sciences, Shanghai 201203, China*

ARTICLE INFO

Article history:
Received 23 September 2024
Revised 17 December 2024
Accepted 26 January 2025
Available online 20 August 2025

Keywords:
Aconiti Lateralis Radix Praeparata
Diterpenoid alkaloids
Processing
Untargeted metabolomics
Mass spectrometry imaging

ABSTRACT

Aconiti Lateralis Radix Praeparata (Fuzi) represents a significant traditional Chinese medicine (TCM) that exhibits both notable pharmacological effects and toxicity. Various processing methods are implemented to reduce the toxicity of raw Fuzi by modifying its toxic and effective components, primarily diterpenoid alkaloids. To comprehensively analyze the chemical variations between different Fuzi products, ultra-high performance liquid chromatography-linear ion trap quadrupole Orbitrap mass spectrometry (UHPLC-LTQ-Orbitrap MS) was employed to systematically characterize Shengfuzi, Heishunpian and Baifupian. A total of 249 diterpenoid alkaloids present in Shengfuzi were identified, while only 111 and 61 in Heishunpian and Baifupian were detected respectively, indicating substantial differences among these products. An untargeted metabolomics approach combined with multivariate statistical analysis revealed 42 potential chemical markers. Through subsequent validation using 52 batches of commercial Heishunpian and Baifupian samples, 8 robust markers distinguishing these products were identified, including AC1-propanoic acid-3OH, HE-glucoside, HE-hydroxyvaleric acid-2OH, dihydrosphingosine, *N*-dodecoxycarbonylvaline and three unknown compounds. Additionally, the MS imaging (MSI) technique was utilized to visualize the spatial distribution of chemical constituents in raw Fuzi, revealing how different processing procedures affect the chemical variations between Heishunpian and Baifupian. The distribution patterns of different diterpenoid alkaloid subtypes partially explained the chemical differences among products. This research provides valuable insights into the material basis for future investigations of different Fuzi products.

1. Introduction

Aconiti Lateralis Radix Praeparaia, known as Fuzi in China, comprises the processed products of the lateral roots of *Aconitum carmichaelii* and has been utilized for thousands of years to rescue patients from collapse, disperse cold, and alleviate pain [1]. Contemporary research confirms Fuzi's broad pharmacological activities, including cardiac, anti-arrhythmic, anti-inflammatory, analgesic, anti-tumor, and other effects [2]. In certain regions of China, people consume medicinal liquors containing Fuzi or prepare Fuzi with meat as a health-promoting food [3]. However, its high toxicity and narrow therapeutic window have been linked to adverse effects across the cardiovascular, nervous, digestive, and reproductive systems, thereby restricting its clinical utility [4].

Various processing methods (Paozhi) are employed to reduce the toxicity while maintaining the effectiveness of raw Fuzi (Shengfuzi), with black slices (Heishunpian) and white slices (Baifupian) being the two most commonly used processed products in clinical practice [5]. According to the *Chinese Pharmacopeia* (2020 Edition), the primary processing procedures for Heishunpian involve washing the raw materials, soaking in Danba (the edible mother liquor of mineral salt preparation), thorough boiling, water rinsing, longitudinal cutting into 0.5 cm thick slices, water soaking and rinsing, staining, steaming, and drying. The processing procedures for Baifupian follow a similar pattern, except for peeling before cutting into 0.3 cm thick slices and steaming without staining, potentially resulting in distinct chemical compositions and variations in effectiveness and toxicity.

Diterpenoid alkaloids, particularly those of the C19 and C20 types, are recognized as the principal active and toxic constituents of Fuzi [6,7]. C20-type diterpenoid alkaloids are structurally diverse and include subtypes such as napelline-, artisine-, and hetisine-type alkaloids. C19-type diterpenoid alkaloids are further

* Corresponding author.
E-mail addresses: zhangtongshutcm@hotmail.com (T. Zhang); daguo@simm.ac.cn (D. Guo)

https://doi.org/10.1016/S1875-5364(25)60936-8

classified based on their substituents: amino alcohol-type (C19-ADAs) lacking ester groups; monoester-type (C19-MDAs) with a single ester group; diester-type (C19-DDAs) containing two ester groups; and lipo-type (C19-LDAs), featured with medium- to long-chain fatty acid esters. During traditional processing, toxic C19-DDAs, such as aconitine, mesaconitine, and hypaconitine, are hydrolyzed into less toxic derivatives. These include C19-MDAs (e.g., benzoylaconine, benzoylmesaconine, benzoylhypaconine) and C19-ADAs (e.g., aconine, mesaconine, hypaconine) [8]. Additionally, complex chemical reactions such as lipid exchange may generate C19-LDAs during processing [9]. These modifications significantly alter the profiles of both toxic and pharmacologically active compounds in Fuzi [10], highlighting the need for further investigation into their implications for safety and efficacy.

Currently, liquid chromatography-mass spectrometry (LC-MS) serves as an effective tool for analyzing complex constituents in traditional Chinese medicines (TCMs) by combining liquid chromatography's separation capacity with MS's selectivity and sensitivity [11]. Through the integration of various data acquisition and post-processing methods, including dynamic exclusion (DE), precursor ion list (PIL), mass defect filtering (MDF), neutral loss filtering (NLF), diagnostic ion filtering (DIF), and others, additional similar or novel components can be identified in TCMs such as Fuzi using LC-MS [12]. However, since the *in situ* distribution of components in tissues may correlate with processing procedures such as peeling of Baifupian, samples for LC-MS analysis require extraction, potentially losing this information. MS imaging (MSI) represents an advanced imaging technique that integrates MS's ion scanning process with specialized image processing software to analyze the chemical composition, relative abundance, and spatial distribution of multiple molecules on a sample surface, without requiring radioisotope or fluorescent labeling [13]. It enables the detection of distribution characteristics and content changes of genes, proteins, and drugs in different physiological and pathological processes, offering significant potential in clinical medicine, molecular biology, and pharmacy. Recent years have seen its widespread applications in medicinal plant analysis for visualization of natural products *in situ*, exploration of biosynthetic pathways, and discovery of new natural products [14]. For instance, desorption electrospray ionization (DESI)-MSI combined with metabolomics-based multivariate statistical analysis has been employed to visualize chemical changes and screen potential metabolic markers of *Aconitum* alkaloids among raw and processed Fuzi with different steaming times, offering an efficient approach to ensure the safety of Fuzi and other toxic TCMs [15]. An UPLC-Q-TOF-MS-based metabolomics method integrated with DESI-MSI was utilized to characterize chemical variations in Tiebangchui and its Zanba processed products, demonstrating significant potential in process monitoring and safety control of Tiebangchui and other toxic *Aconitum* medicine [16].

In this investigation, ultra-high performance liquid chromatography-linear ion trap quadrupole Orbitrap MS (UHPLC-LTQ-Orbitrap MS) was employed to systematically characterize diterpenoid alkaloids in Shengfuzi, Heishunpian, and Baifupian, comparing the quantities of different diterpenoid alkaloid subtypes in these products. Integration with MDF data post-processing enabled the discovery of additional potential diterpenoid alkaloids with novel structures while filtering out interfering ions. Furthermore, an untargeted metabolomics approach combined with multivariate statistical analysis was implemented to compare chemical constituents in Heishunpian and Baifupian and identify distinguishing chemical markers. Subsequently, 52 batches of commercial samples were analyzed to validate these markers and identify robust chemical markers, establishing a foundation for understanding the chemical and pharmacological differences between these Fuzi products. Additionally, given the distinct processing steps of Heishunpian and Baifupian such as peeling, the MSI technique was utilized to visualize the spatial distribution of different diterpenoid alkaloid subtypes in raw Fuzi, revealing potential factors contributing to chemical differences between Heishunpian and Baifupian, thus providing valuable insights for developing appropriate Fuzi processing procedures from a material basis.

2. Materials and methods

2.1. Chemicals and reagents

The raw materials of Fuzi for MSI analysis were collected from Jiangyou, Sichuan Province, China, and authenticated by Prof. Dean Guo (Shanghai Institute of Materia Medica, Chinese Academy of Sciences). A voucher specimen was deposited in the National Engineering Research Center for TCM Standardization Technology, Shanghai Institute of Materia Medica, Chinese Academy of Sciences, Shanghai, China. Eleven batches of Shengfuzi (S) were obtained from Jiangyou, Sichuan Province, China. Additionally, 28 batches of processed products comprising 13 batches of Heishunpian (H) and 15 batches of Baifupian (B) were processed by Yichun Wujiashen Pharmaceutical Co., Ltd. (Yichun, China). Furthermore, 52 batches of commercial samples, including 26 batches of Heishunpian (GH) and 26 batches of Baifupian (GB) were sourced from different GMP manufacturers. The representative images of Shengfuzi, Heishunpian and Baifupian are shown in Supporting Fig. S1. Forty-four diterpenoid alkaloids served as reference standards for systematic characterization of Fuzi, isolated and identified by the author as described in a previous study [7], with their identities and structures presented in Supporting Table S1 and Fig. S2. Methanol and formic acid of analytical grade were acquired from Sinopharm Chemical Reagent Co., Ltd. (Shanghai, China). LC-MS grade acetonitrile (J&K Scientific Ltd., Beijing, China; ACN) and formic acid (Shanghai Aladdin Biochemical Technology Co., Ltd., Shanghai, China; FA) were utilized for LC-MS analysis. The deionized water was prepared using a Millipore Alpha-Q water purification system (Millipore, Bedford, USA).

2.2. Sample preparation

Sample solutions for UHPLC-LTQ-Orbitrap MS analysis were prepared by adding 1 mL of 75% aqueous methanol (containing 0.1% FA) to 100 mg of the fine sample powder of each batch of Fuzi, sonicated on a water bath (37 kHz, 1130 W) at room temperature for 30 min, and then centrifuged at 14 000 $r \cdot min^{-1}$ for 10 min. The supernatant was collected as the sample solution for metabolomic analysis. Additionally, each group of sample solutions was combined to obtain three mixed sample solutions for systematic characterization. These mixed sample solutions were further combined to create a QC sample solution to evaluate the system stability of the untargeted metabolomics method.

Sample slices for MSI analysis were prepared by washing the fresh raw materials of Fuzi with deionized water, cutting them transversely into small pieces of approximately 2 cm in diameter with a knife, and embedding them with carboxymethyl cellulose sodium (CMC-Na). The embedded tissues were sectioned at 100 μm using a Leica CM1950 cryostat (Leica Mikrosysteme Vertrieb GmbH, Wetzlar, Germany) with the chamber temperature maintained at −15 °C. The obtained slices were attached to glass slides with double-adhesive tapes and stored at −20 °C prior to analysis.

2.3. UHPLC-LTQ-Orbitrap MS and MSI methods

UHPLC-LTQ-Orbitrap MS analysis was conducted using a

Thermo Scientific UltiMate 3000 UHPLC chromatographic system and a Thermo Scientific LTQ-Orbitrap Velos Pro hybrid mass spectrometer with Xcalibur 2.1 software (Thermo Fisher Scientific, San Jose, CA, USA) for instrument control and data processing. Chromatographic separation was performed on a Waters ACQUITY UPLC CSH C_{18} column (2.1 mm × 100 mm, 1.7 μm; Waters Corporation, Milford, MA, USA) at 30 °C and eluted with the binary mobile phase comprising solvent A (0.1% formic acid in water, *V*/*V*) and solvent B (acetonitrile) at a flow rate of 0.3 mL·min^{-1} with the following gradient: 0–4 min, 5%–8% B; 4–10 min, 8%–18% B; 10–15 min, 18%–30% B; 15–20 min, 30%–40% B; 20–25 min, 40%–100% B; 25–30 min, 100% B. The injection volume was 1 μL, and the PDA detector was set between 190 and 400 nm and at 235 nm. Mass spectrometry was conducted in positive ion mode, and the ESI source parameters were configured as follows: ion source voltage, 3.8 kV; capillary temperature, 350 °C; source heater temperature, 300 °C; sheath gas (N_2), 40 arbitrary units; auxiliary gas (N_2), 10 arbitrary units; sweep gas (N_2), 2 arbitrary units. For the characterization of diterpenoid alkaloids, multistage MS data was acquired in collision-induced dissociation (CID) mode at normalized collision energy (NCE) of 35% and three events. Event 1 was a full scan with a mass range of *m*/*z* 100–1000, at the resolution of 30,000 in profile data format. Events 2 and 3 triggered the fragmentations of the most intense ions of the former event respectively at the resolution of 7500 in centroid format. The minimum signal intensity to trigger MS^2 and MS^3 fragmentations were 5000 and 500, respectively. DE parameters were configured as follows: repeat count, 2; repeat duration, 10 s; exclusion list size, 50; exclusion duration, 10 s; low or high exclusion mass width, 1.5 Da. For untargeted metabolomics study, data was acquired in full scan mode with a mass range of *m*/*z* 100–1000 at the resolution of 30 000 in profile data format.

MSI analysis was performed using a Waters Synapt G2-S QTof mass spectrometer equipped with a DESI source (Waters Corporation, Milford, MA, USA). Methanol served as the spray solvent at a flow rate of 2 μL·min^{-1}. The ionization mode was positive, the capillary voltage was 3.5 kV, and the spatial resolution (pixel size) was 50 μm. A mass range of *m*/*z* 50–1200 and a scan rate of 50 μm·s^{-1} were utilized for imaging. Data was acquired using MassLynx 4.1 software (Waters Corporation, Milford, MA, USA). Data acquisition setup, processing, and visualization were conducted using HDI 1.4 software (Waters Corporation, Milford, MA, USA).

2.4. Data processing methods

Compound Discoverer 3.1 software (Thermo Fisher Scientific, San Jose, CA, USA) was employed for peak picking of the ions acquired by MS for characterization. Additionally, an MDF method, established in our previous study using Eqs. (1)–(4) [12], was applied to process both the MS data acquired for characterization and untargeted metabolomics analysis for filtering of all potential ions of diterpenoid alkaloids, in which mass defects (mDa; *y*) referred to the decimal parts of their *m*/*z* ($[M + H]^+$) values and mass ranges (Da; *x*) were their integer parts with even numbers from 298 to 1020 Da.

$$0.2793x + 42.741 < y < 0.2793x + 236.795 \quad (1)$$

$$-3.5804x + 1284.0592 < y < -3.5804x + 4168.804 \quad (2)$$

$$0.3228x + 222.5216 < y < 0.3228x + 323.9744 \quad (3)$$

$$-3.0979x + 2914.0704 < y < -3.0979x + 3409.7596 \quad (4)$$

The untargeted metabolomics data were processed using Progenesis QI v2.3 software (Nonlinear Dynamics, Newcastle, UK), which performed automatic peak alignment, peak picking, deconvolution, and normalization. The analysis parameters specified $[M + H]^+$ as the possible adduction form, with a time range of 0–30 min. Subsequently, ions with odd *m*/*z* values were eliminated, and ions showing RSD > 30% of normalized abundance in QC samples were removed to ensure data stability and repeatability. Additionally, the established MDF method [Eqs. (1)–(4)] was applied to filter potential diterpenoid alkaloid ions.

3. Results and discussion

3.1. Systematic characterization of diterpenoid alkaloids in Fuzi

To investigate the chemical differences among various processed products of Fuzi, diterpenoid alkaloids in Shengfuzi, Heishunpian and Baifupian underwent systematic characterization. The analysis incorporated 44 reference standards (Table S1 and Fig. S1) previously isolated and identified by the author [7] for compound comparison. An in-house library developed using Compound Discoverer 3.1 software [12], containing compound name, type, molecular formula, molecular weight, and chemical structure information, facilitated rapid matching of known compounds. Furthermore, an MDF method was implemented to filter potential diterpenoid alkaloid ions while eliminating interference [12]. Through comparison of MS information (including *m*/*z* value, retention time, precursor ion, and fragmentation ions) with reference compounds, the in-house library, and online databases (SciFinder, Reaxys, PubChem), 249 components were characterized across different processed products (Table S2). These included 182 C19-diterpenoid alkaloid subtypes, 37 C20-diterpenoid alkaloid subtypes, and 30 unknown components requiring further identification through techniques such as nuclear magnetic resonance (NMR). The findings demonstrated LC-MS as both an efficient method for rapid characterization of predicted compounds and a powerful tool for discovering novel components with unique substituents or nuclei in complex systems. Figs. S3-S5 illustrated the core structures of different diterpenoid alkaloid subtypes, fragment ions, and pathways of representative compounds, while Fig. 1 presented the base peak chromatograms of the three processed products.

The characterization results revealed that all 249 components were detectable in Shengfuzi (S), while Heishunpian (H) and Baifupian (B) contained 111 and 61 components, respectively. Analysis of different diterpenoid alkaloid subtypes across products (Fig. 2) indicated that all subtypes decreased or disappeared during processing from Shengfuzi to Heishunpian or Baifupian, attributable to both chemical transformations and component loss during processing steps such as water soaking and rinsing. Heishunpian exhibited more detectable diterpenoid alkaloids than Baifupian, including C19-ADAs, C19-MDAs, C19-LDAs, and C20-type diterpenoid alkaloids. However, the number of C19-DDAs remained similar between them, suggesting comparable toxicity but potentially different bioactivity.

Historical medical texts, including *Treatise on Febrile Diseases* (*Shanghanlun*), document distinct applications for Baifupian and Heishunpian. Baifupian, prepared by removing the skin, was traditionally prescribed for milder conditions such as extremity pain, cold-induced constipation, and laryngeal obstruction. In contrast, Heishunpian was indicated for more severe conditions, including emesis, gastric reflux, cardiac pain, and stroke-induced hemiplegia. In contemporary medicine, both preparations are utilized for treating acute myocardial infarction, coronary heart disease, and chronic heart failure, without strict clinical differentiation [4, 17]. Research has demonstrated that C19-MDAs, C19-ADAs, and certain C20 diterpenoid alkaloids like songorine [18] possess anti-inflammatory, analgesic, and immunomodulatory properties. Studies [19] have confirmed superior analgesic and anti-

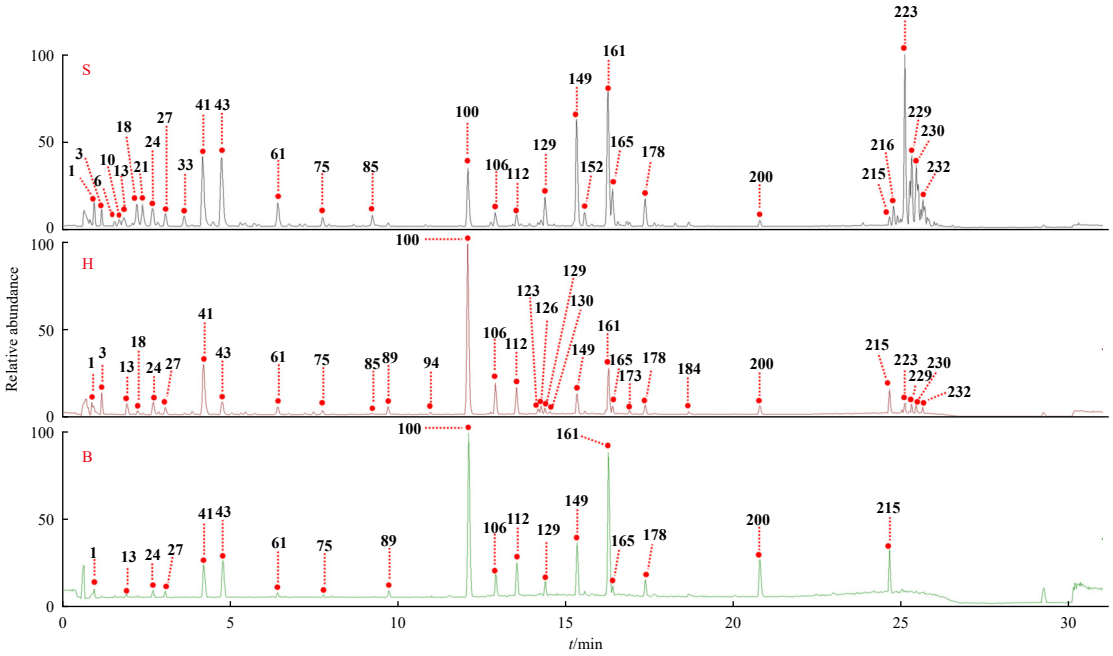

Fig. 1 The base peak chromatograms of Shengfuzi (S), Heishunpian (H), and Baifupian (B).

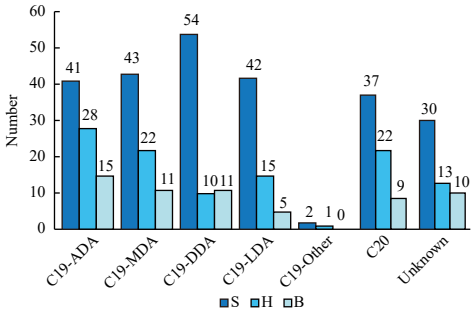

Fig. 2 The subtype classification of the characterized diterpenoid alkaloids in Shengfuzi (S), Heishunpian (H), and Baifupian (B).

inflammatory effects of Heishunpian compared to Baifupian, supporting both traditional clinical distinctions and the chemical compositional differences identified in this study. Regarding toxicology, with C19-DDAs being the primary toxic components in Fuzi, previous research [20] established the LD_{50} values for mice treated with Heishunpian and Baifupian extracts at 49.853 and 42.550 g crude drug·kg^{-1} respectively, showing no significant differences, which aligns with our findings.

Compounds **13** (*m/z* 486.2689, t_R 1.81 min) and **20** (*m/z* 360.2523, t_R 2.22 min) serve as representative examples for the structure elucidation of C19-ADAs. For compound **13**, the molecular formula was determined to be $C_{24}H_{39}O_9N$, with the molecular ion of *m/z* 486.2689 ($[M + H]^+$) initially observed in the CID-MS^1 spectrum. The subsequent loss of one H_2O molecule and one CH_3OH molecule yielded a fragment ion of *m/z* 436.2339 ($[M + H - H_2O - CH_3OH]^+$) in the CID-MS^2 spectrum. Further sequential or concurrent neutral losses (NL) of H_2O and CH_3OH produced fragment ions of *m/z* 404.2070 ($[M + H - H_2O - 2CH_3OH]^+$), *m/z* 386.1966 ($[M + H - 2H_2O - 2CH_3OH]^+$), *m/z* 372.1808 ($[M + H - H_2O - 3CH_3OH]^+$), *m/z* 354.1705 ($[M + H - 2H_2O - 3CH_3OH]^+$), *m/z* 336.1583 ($[M + H - 3H_2O - 3CH_3OH]^+$), *m/z* 322.1434 ($[M + H - 2H_2O - 4CH_3OH]^+$) and *m/z* 304.1334 ($[M + H - 3H_2O - 4CH_3OH]^+$) in the CID-MS^3 spectrum, indicating hydroxyl group (NL H_2O) and methoxyl groups (NL CH_3OH) substituents in the nucleus. Through comparison with the reference standard and in-house library, compound **13** was identified as mesaconine. For compound **20**, the protonated molecular ion of *m/z* 360.2523 ($[M + H]^+$) was detected in the CID-MS^1 spectrum. The product ions of *m/z* 342.2438 ($[M + H - H_2O]^+$, *m/z* 324.3325 ($[M + H - 2H_2O]^+$), *m/z* 310.2172 ($[M + H - H_2O - CH_3OH]^+$) and *m/z* 292.2063 ($[M + H - 2H_2O - CH_3OH]^+$) were generated in CID-MS^2 and CID-MS^3 spectra through sequential or simultaneous NL of two H_2O molecules and one CH_3OH molecule, suggesting two hydroxyl groups (OH) and one methoxyl group (OMe) substitutions in the nucleus. The molecular formula $C_{22}H_{33}O_3N$ suggested that the compound possesses a dehydrogenated AC3-type core, representing a novel structural variant arising from the oxidative modification of the AC3 nucleus. Consequently, compound **20** was characterized as dehydro-AC3-OMe-2OH.

Compounds **55** (*m/z* 450.2841, t_R 5.70 min) and **112** (*m/z* 574.3007, t_R 13.50 min) serve as representative examples for elucidating the structure of C19-MDAs. In positive ion mode, the precursor ions of compounds **55** and **112** exhibited *m/z* values of 450.2841 and 574.3007, respectively, corresponding to molecular formulas of $C_{25}H_{39}O_6N$ and $C_{31}H_{43}O_9N$. For compound **55**, the CID-MS^2 spectrum revealed an NL of H_2O, yielding the base peak ion $[M + H - H_2O]^+$ (*m/z* 432.2755). The CID-MS^3 spectrum showed subsequent NL of CH_3COOH, CH_3OH, and H_2O, generating ions at $[M + H - H_2O - CH_3COOH]^+$ (*m/z* 372.2533), $[M + H - H_2O - CH_3COOH - CH_3OH]^+$ (*m/z* 340.2272), $[M + H - H_2O - CH_3COOH - 2CH_3OH]^+$ (*m/z* 308.2015), and $[M + H - 2H_2O - CH_3COOH - 2CH_3OH]^+$ (*m/z* 290.1909). These fragmentations indicate the presence of hydroxyl groups (OH, NL H_2O), acetyl group (OAc, NL $C_2H_4O_2$), and methoxyl groups (OMe, NL CH_3OH) in the nucleus. Through comparison with the reference standard and in-house library, compound **55** was identified as condelphine. For compound **112**, the CID-MS^2 and CID-MS^3 spectra demonstrated NL of CH_3OH, $C_7H_6O_2$, and H_2O, producing fragment ions at $[M + H - OH]^+$ (*m/z* 542.2762), $[M + H - CH_3OH - C_7H_6O_2]^+$ (*m/z* 420.2385), $[M + H - CH_3OH - C_7H_6O_2 - H_2O]^+$ (*m/z* 402.2290), $[M + H - 2CH_3OH - C_7H_6O_2 - H_2O]^+$ (*m/z* 370.2015), $[M + H - 3CH_3OH - C_7H_6O_2 - H_2O]^+$ (*m/z* 338.1756), $[M + H - 4CH_3OH - C_7H_6O_2 - H_2O]^+$ (*m/z* 306.1496), and $[M + H - 4CH_3OH - C_7H_6O_2 - 2H_2O]^+$ (*m/z* 288.1398). These fragmentations indicate the presence of methoxyl groups (OMe, NL CH_3OH), benzoyl group (OBz, NL $C_7H_6O_2$), and hydroxyl groups (OH, NL H_2O) in the nucleus. Through comparison with the reference standard

and in-house library, compound **112** was identified as benzoylhypaconine.

Compounds **149** (*m/z* 632.3045, t_R 15.28 min) and **153** (*m/z* 702.3108, t_R 15.62 min) serve as representative examples for elucidating the structure of C19-DDAs. Their molecular formulas were determined as $C_{33}H_{45}O_{11}N$ and $C_{36}H_{47}O_{13}N$, respectively. In the CID-MS^2 spectrum, NL of CH_3COOH or $C_5H_6O_4$ generated diagnostic ions $[M + H - CH_3COOH]^+$ (*m/z* 572.2874) or $[M + H - C_5H_6O_4]^+$ (*m/z* 572.2846), indicating acetyl group substitution (NL CH_3COOH) in compound **149** and glutaconic acid group substitution in compound **153**. For compound **149**, subsequent NL of $C_7H_6O_2$, CH_3OH and H_2O in the CID-MS^3 spectrum produced ions $[M + H - CH_3COOH - C_7H_6O_2]^+$ (*m/z* 450.2506), $[M + H - CH_3COOH - C_7H_6O_2 - CH_3OH]^+$ (*m/z* 418.2233), $[M + H - CH_3COOH - C_7H_6O_2 - 2CH_3OH]^+$ (*m/z* 386.1970), $[M + H - CH_3COOH - C_7H_6O_2 - 3CH_3OH]^+$ (*m/z* 354.1708), $[M + H - CH_3COOH - C_7H_6O_2 - 3CH_3OH - H_2O]^+$ (*m/z* 336.1605), and $[M + H - CH_3COOH - C_7H_6O_2 - 4CH_3OH]^+$ (*m/z* 322.1459), indicating the presence of benzoyl group (NL $C_7H_6O_2$), methoxyl groups (NL CH_3OH) and hydroxyl groups (NL H_2O). Through comparison with the reference standard and in-house library, compound **149** was identified as mesaconitine. Compound **153** exhibited similar fragment ions in its CID-MS^3 spectrum to compound **149**, with the main structural difference being the substitution of a glutaconic acid group instead of an acetyl group at the C-8 position. Consequently, compound **153** was characterized as 8-*O*-glutaconic acid-benzoylmesaconine.

Compound **113** (*m/z* 928.3941, t_R 13.62 min) serves as an example for elucidating the structure of C19-LDAs. C19-LDAs represent a distinct subclass of C19-DDAs, characterized by C-8 position substitution with medium to long chain fatty acid ester groups containing 6 or more carbon atoms, while the C-14 position typically features a benzoyl group ($OCOC_6H_5$). Compound **113**, with molecular formula $C_{47}H_{61}O_{18}N$, exhibited an NL of $C_{16}H_{20}O_9$ in its CID-MS^2 spectrum, corresponding to a novel 2-β-D-glucopyranosyloxy-4-methoxycinnamic acid substituent or similar structures, yielding the base peak ion $[M + H - C_{16}H_{20}O_9]^+$ (*m/z* 572.2864). Subsequent NL of CH_3OH, $C_7H_6O_2$, and H_2O in the CID-MS^3 spectrum generated fragment ions similar to those of compounds **149** and **153**. Thus, compound **113** was identified as AC2-$OC_{16}H_{19}O_8$-benzoylmesaconine.

Compounds **27** (*m/z* 360.2519, t_R 2.77 min) and **6** (*m/z* 378.2638, t_R 1.53 min) demonstrate the structure elucidation process for C20-type diterpenoid alkaloids. Compound **27**, with molecular formula $C_{22}H_{33}O_3N$, displayed the NL of three H_2O molecules in its CID-MS^2 and CID-MS^3 spectra, producing fragment ions $[M + H - H_2O]^+$ (*m/z* 342.2432), $[M + H - 2H_2O]^+$ (*m/z* 324.2330), and $[M + H - 3H_2O]^+$ (*m/z* 306.2225), indicating three hydroxyl group substitutions in the nucleus. Through comparison with the reference standard and in-house library, compound **27** was identified as napelline, a napelline-type C20 diterpenoid alkaloid. Compound **6**, with molecular formula $C_{22}H_{35}O_4N$, exhibited NL of four H_2O molecules in its CID-MS^2 and CID-MS^3 spectra, generating fragment ions $[M + H - H_2O]^+$ (*m/z* 360.2542), $[M + H - 2H_2O]^+$ (*m/z* 342.2430), $[M + H - 3H_2O]^+$ (*m/z* 324.2327), and $[M + H - 4H_2O]^+$ (*m/z* 306.2218), indicating four hydroxyl group substitutions in the nucleus. Therefore, compound **6** was identified as AT-4OH, a member of the artisine-type C20 diterpenoid alkaloids bearing four hydroxyl substitutions.

3.2. Discovery of the potential markers by multivariate statistical analysis

To investigate the chemical differences among various processed products of Fuzi, an untargeted metabolomics study was conducted. The LTQ-Orbitrap MS was employed for data acquisition of sample solutions from 11 batches of Shengfuzi (S), 13 batches of Heishunpian (H), and 15 batches of Baifupian (B) in a randomized order. To ensure the reliability of the analytical results, QC samples were injected after every 8–10 experimental runs. The resulting LC-MS data were processed using Progenesis QI v2.3 software, applying the MDF method outlined in section 2.3. This approach generated a dataset comprising 6720 ions, each annotated with *m/z* value, retention time, and ion intensity, potentially corresponding to diterpenoid alkaloids. These ion features were then subjected to multivariate statistical analysis using SIMCA 14.1 software (Umetrics, Umeå, Sweden), employing principal component analysis (PCA) for pattern recognition and orthogonal partial least squares discriminant analysis (OPLS-DA).

The PCA score plot (Fig. 3) demonstrated that the QC samples clustered effectively, indicating system stability during continuous injections and confirming data reliability. Additionally, Shengfuzi, Heishunpian and Baifupian formed distinct clusters, with the Shengfuzi cluster notably separated from the Heishunpian and Baifupian clusters, suggesting substantial differences between the chemical compositions of Shengfuzi and these two products, but minimal differences between Heishunpian and Baifupian, consistent with the findings in section 3.1.

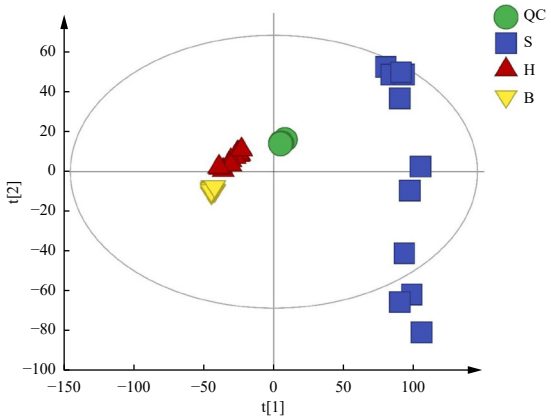

Fig. 3 The PCA score plot of Shengfuzi (S), Heishunpian (H), and Baifupian (B).

To elucidate the chemical distinctions between Heishunpian and Baifupian and identify potential differential chemical markers, OPLS-DA was conducted, with the score plot presented in Fig. 4A. R^2 and Q^2 values of this model were 0.777 and 0.64, respectively, demonstrating good stability and prediction ability. The results of 200 perturbation tests showed that all R^2 and Q^2 points on the left were lower than the original points on the right, and the blue regression line of the Q^2 points intersected the vertical axis below zero, confirming the model was not overfitting and the predictions were reliable. The VIP score plot was generated (Fig. 4B), and 378 components with VIP values exceeding 1 were identified as potential differential components. The volcano plot (Fig. 4B) showed components with $P < 0.05$ and $FC > 2$ (or < 0.5) were significantly increased (or decreased) in Baifupian compared to Heishunpian. In total, 223 components were identified, including 138 down-regulated and 85 up-regulated components in Baifupian compared to Heishunpian. The heatmap (Fig. 4C) visualized the relative contents of these components.

3.3. Validation of robust chemical markers with commercial samples

A total of 52 commercial samples comprising 26 batches of Heishunpian (GH) and 26 batches of Baifupian (GB) were analyzed to validate the 223 differential chemical markers identified in section 3.2. Full scan MS data for each sample was obtained using UHPLC-LTQ-Orbitrap MS and processed with Progenesis QI v2.3 software. Subsequently, 42 compounds with $P < 0.05$ of the

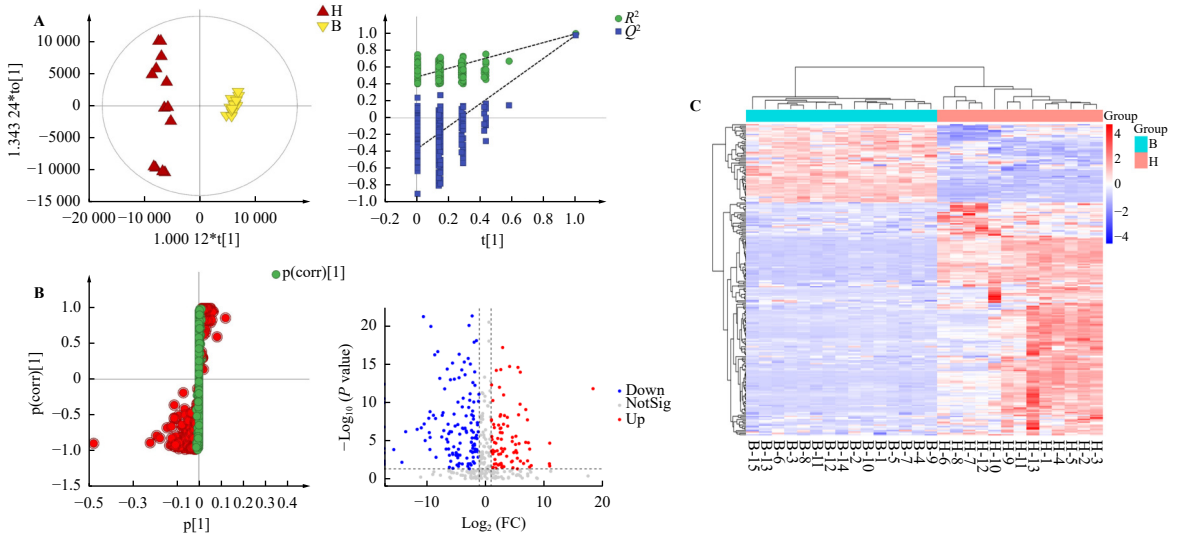

Fig. 4 A, The OPLS-DA score plot and permutation test of Heishunpian (H) and Baifupian (B). B, The VIP score plot and volcano plot of Heishunpian (H) and Baifupian (B). C, The cluster heatmap of the differential components between Heishunpian (H) and Baifupian (B).

normalized abundance were selected for further validation. The PCA score plot (Fig. 5A) generated using SIMCA-P 14.1 software revealed that GH and GB samples could not be fully distinguished using these compounds, potentially due to variations among commercial samples resulting from diverse processing procedures across manufacturers.

To identify biomarkers capable of distinguishing GH and GB samples, ion abundance variations were examined across a comprehensive set of specimens. This dataset included 28 batches of laboratory-prepared H and B samples (as detailed in section 3.2), along with 52 batches of commercially sourced counterparts. Scatter plots were constructed to visualize the distribution of ion intensities across all sample groups (Fig. S6). Eight compounds (Table S3) exhibiting significant abundance differences between Heishunpian and Baifupian were identified and characterized as AC1-propanoic acid-3OH (m/z 392.2415, t_R 4.54 min), HE-glucoside (m/z 460.2691, t_R 4.60 min), HE-hydroxyvaleric acid-2OH (m/z 430.2588, t_R 5.44 min), dihydrosphingosine (m/z 302.3053, t_R 23.27 min), *N*-dodecoxycarbonylvaline (m/z 394.3299, t_R 27.07 min) and three unknown compounds (m/z 404.3372, t_R 24.40 min; m/z 786.3116, t_R 24.68 min; m/z 468.2744, t_R 24.87 min) requiring further identification through techniques such as NMR. The PCA score plot (Fig. 5B) based on these eight compounds demonstrated the effective distinction between most GH and GB samples, establishing their utility as robust chemical markers for differentiating commercial Heishunpian and Baifupian samples.

3.4. Spatial distribution of diterpenoid alkaloids by MSI

This study has demonstrated significant chemical constituent differences between Heishunpian and Baifupian. Given that their primary processing difference involves peeling, the compounds distributed in different Fuzi tissue regions, particularly the cortex, may influence their chemical variations. Since LC-MS analysis requires sample homogenization for extraction, making it challenging to correlate compound content and distribution with Fuzi botanical structures, the MSI technique was employed to visualize the *in situ* spatial distribution of different diterpenoid alkaloid subtypes in raw Fuzi.

Sample preparation significantly influences the authenticity and accuracy of MSI results, correlating with analyst properties, sample types, and conditions. Plant tissue sample preparation presents greater challenges compared to animal tissues. As

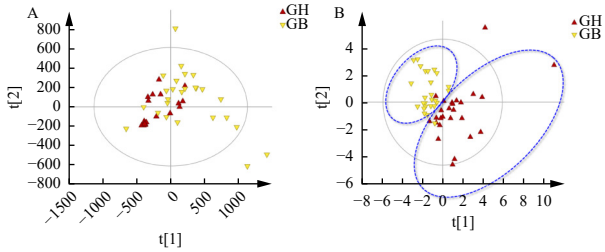

Fig. 5 (A) The PCA score plot of 42 markers to distinguish commercial samples. (B) The PCA score plot of 8 robust markers to distinguish commercial samples.

frozen plant tissues are loose, brittle, and prone to folding, maintaining sample integrity and tissue surface flatness is crucial [21]. The sample preparation method was optimized to preserve raw Fuzi sample integrity, focusing primarily on section temperature and thickness. Raw Fuzi samples became excessively hard at −20 °C and too soft at room temperature, both unsuitable for frozen slice preparation. The optimal section temperature was determined to be −15 °C, providing moderate hardness suitable for sectioning. Furthermore, sections thinner than 100 μm were prone to damage, compromising integrity. At 100 μm thickness, samples maintained completeness and demonstrated good ion response in imaging results, thus 100 μm was established as the optimal section thickness.

The spatial distribution of each component was analyzed using MSI data from Fuzi slices, with subtypes identified through comparison with characterization results from section 3.1. The Fuzi slice optical image (Fig. 6A) reveals transverse section structures, including cortex, phloem, xylem, and pith. MSI results (Figs. 6B–6D) demonstrated distinct distribution patterns for each compound, with yellow indicating relatively higher concentrations and black indicating lower concentrations. Most C19-DDAs showed widespread distribution throughout Fuzi slices with minor variations: components such as hypaconitine, beiwutine, and aconifine exhibited higher concentrations in the cortex and phloem compared to the pith; aconitine showed higher content in the pith than phloem; mesaconitine distributed evenly between pith and phloem but not cortex; while deoxyaconitine demonstrated uniform distribution throughout the tissue. C19-MDAs are primarily concentrated in the cortex and phloem at low levels. C19-ADAs exhibited irregular spatial distribution patterns: components including senbusine A/B, fuziline, hypaconine, and mesaconine concentrated mainly in the cortex and phloem; car-

michaenine B and 8-dehydroxyl-bikhaconine distributed evenly throughout the section; while aconine primarily concentrated in the pith.

The results revealed that C19-DDAs exhibited higher concentrations and uniform distribution throughout raw Fuzi tissues, whereas C19-MDAs and C19-ADAs demonstrated lower concentrations with heterogeneous distribution, predominantly in the cortex and phloem regions. These distribution patterns potentially explained the subtype variations of diterpenoid alkaloids in Heishunpian and Baifupian as discussed in section 3.1. Therefore, MSI serves as an effective tool for analyzing the distribution of secondary metabolites in plant tissues, offering valuable insights for optimizing processing methods [14, 15] and quality control of decoction pieces. Additionally, as established in our previous research [10], Fuzi specimens from different cultivation sites showed varying concentrations of diterpenoid alkaloids, influenced by geographical conditions and harvest timing. MSI technology presents potential applications in investigating the dynamic changes and biosynthetic pathways of diterpenoid alkaloids by revealing their distribution patterns in Fuzi from various cultivation sites and harvest periods, thereby establishing a scientific foundation for future research on efficacy and toxicity variations among different Fuzi sources.

4. Conclusion

This investigation employed UHPLC-LTQ-Orbitrap MS to analyze the chemical differences among various Fuzi products, specifically Shengfuzi, Heishunpian, and Baifupian. A total of 249 diterpenoid alkaloids were identified, revealing substantial variations in alkaloid subtypes across different Fuzi products. An untargeted metabolomics approach, combined with multivariate statistical analysis, was utilized to discover 42 potential chemical markers, showing significant content differences between Heishunpian and Baifupian, from which 8 robust markers were validated and selected for differentiation. Additionally, MSI technology enabled visualization of spatial distribution of chemical components in raw Fuzi slices, providing insight into the subtype variations of diterpenoid alkaloids in differently processed Fuzi, thus offering valuable reference for future development of appropriate Fuzi processing methods.

Funding

This work was supported by the Qi-Huang Chief Scientist Program of the National Administration of Traditional Chinese Medicine (2020), the National Key Research and Development Program of China (No. 2022YFC3501705), Shanghai Sailing Program (No. 23YF1447500), and the China Postdoctoral Science Foundation (No. 2023M732335).

Availability of supporting information

Supporting information of this paper can be requested by sending E-mail to the corresponding author.

Declaration of competing interest

The authors declare that they have no competing interests.

References

1 *Pharmacopoeia of the Peoples Republic of China*. Beijing: People's Medical Publishing House. 2020;1:200-201.
2 Zhou GH, Tang LY, Zhou XD, et al. A review on phytochemistry and pharmacological activities of the processed lateral root of *Aconitum carmichaelii* Debeaux. *J Ethnopharmacol*. 2015;160:173-193. https://doi.org/10.1016/j.jep.2014.11.043.
3 Wang M, Hu WJ, Zhou X, et al. Ethnopharmacological use, pharmacology, toxicology, phytochemistry, and progress in Chinese crude drug processing of the lateral root of *Aconitum carmichaelii* Debeaux. (Fuzi): a review. *J Ethnopharmacol*. 2023;301:115838. https://doi.org/10.1016/j.jep.2022.115838.
4 Singhuber J, Zhu M, Prinz S, et al. *Aconitum* in traditional Chinese medicine: a valuable drug or an unpredictable risk? *J Ethnopharmacol*. 2009;126:18-30. https://doi.org/10.1016/j.jep.2009.07.031.
5 Liu S, Li F, Li Y, et al. A review of traditional and current methods used to potentially reduce toxicity of *Aconitum* roots in traditional Chinese medicine. *J Ethnopharmacol*. 2017;207:237-250. https://doi.org/10.1016/j.jep.2017.06.038.
6 Wu JJ, Guo ZZ, Zhu YF, et al. A systematic review of pharmacokinetic studies on herbal drug Fuzi: implications for Fuzi as personalized medicine. *Phytomedicine*. 2018;44:187-203. https://doi.org/10.1016/j.phymed.2018.03.001.
7 Yu Y, Wu SF, Zhang JQ, et al. Structurally diverse diterpenoid alkaloids from the lateral roots of *Aconitum carmichaelii* Debx. and their anti-tumor activities based on *in vitro* systematic evaluation and network pharmacology analysis. *RSC Adv*. 2021;11:26594-26606. https://doi.org/10.1039/D1RA04223H.
8 Liu M, Cao Y, Lv DY, et al. Effect of processing on the alkaloids in *Aconitum* tubers by HPLC-TOF/MS. *J Pharm Anal*. 2017;7:170-175. https://doi.org/10.1016/j.jpha.2017.01.001.
9 Wang Y, Shi L, Song F, et al. Exploring the ester-exchange reactions of diester-diterpenoid alkaloids in the Aconite Decoction process by electrospray ionization tandem mass spectrometry. *Rapid Commun Mass Sp*. 2003;17(4):279-284. https://doi.org/10.1002/rcm.914.
10 Yu Y, Yao CL, Zhang JQ, et al. Comprehensive quality evaluation of Aconiti Lateralis Radix Praeparata based on pseudotargeted metabolomics and simultaneous determination of fifteen components, and development of new processed products of black slices with less toxicity. *J Pharmaceut Biomed Anal*. 2023;228:115295. https://doi.org/10.1016/j.jpba.2023.115295.
11 Yu Y, Yao CL, Guo DA. Insight into chemical basis of traditional Chinese medicine based on the state-of-the-art techniques of liquid chromatography-mass spectrometry. *Acta Pharm Sin B*. 2021;11(6):1469-1492. https://doi.org/10.1016/j.apsb.2021.02.017.
12 Yu Y, Yao CL, Wei WL, et al. Integration of offline two-dimensional chromatography and mass defect filtering-based precursor ion list data acquisition for targeted characterization of diterpenoid alkaloids in the lateral roots of *Aconitum carmichaelii*. *J Chromatogr A*. 2022;1684:463554. https://doi.org/10.1016/j.chroma.2022.463554.
13 Buchberger AR, DeLaney K, Johnson J, et al. Mass spectrometry imaging: a review of emerging advancements and future insights. *Anal Chem*. 2018;90(1):240-265. https://doi.org/10.1021/acs.analchem.7b04733.
14 Hou JJ, Zhang ZJ, Wu WY, et al. Mass spectrometry imaging: new eyes on natural products for drug research and development. *Acta Pharmacol Sin*. 2022;43:3096-3111. https://doi.org/10.1038/s41401-022-00990-8.
15 Liu Y, Yang XX, Zhou C, et al. Unveiling dynamic changes of chemical constituents in raw and processed Fuzi with different steaming time points using desorption electrospray ionization mass spectrometry imaging combined with metabolomics. *Front Pharmacol*. 2022;13:842890. https://doi.org/10.3389/fphar.2022.842890.
16 Li CY, Sha MX, Pei ZQ, et al. Dynamic variations in the chemical constituents of Tiebangchui stir-fried with Zanba by integrating UPLC-Q-TOF-MS based metabolomics and DESI-MSI. *Arab J Chem*. 2023;16:104957. https://doi.org/10.1016/j.arabjc.2023.104957.
17 Pu TT, Liu J, Zhou ZY, et al. Differences between processed product Heishunpian and Baifupian using fourier transform infrared spectroscopy and HPLC. *Chin Tradit Herbal Drugs*. 2024;55(2):596-604. https://doi.org/10.7501/j.issn.0253-2670.2024.02.025.
18 Nesterova YV, Povet'yeva TN, Suslov NI, et al. Analgesic activity of diterpene alkaloids from *Aconitum baikalensis*. *Bull Exp Biol Med*. 2014;157(4):488-491. https://doi.org/10.1007/s10517-014-2598-6.
19 Shao F, Li SL, Liu RH, et al. Analgesic and anti-inflammatory effects of different processed products of Aconiti Lateralis Radix Praeparata. *Lishizhen Med Mater Med Res*. 2011;22(10):2329-2330. https://doi.org/10.1111/j.1600-0714.2011.01024.x.
20 Xie XF, Peng C, Yi JH, et al. Comparative study on acute toxicity of extracts from different processed products of Aconiti Lateralis Radix Praeparata. *Pharm Clin Chin Mater Med*. 2012;3(3):29-33,51.
21 Dong YH, Li B, Malitsky S, et al. Sample preparation for mass spectrometry imaging of plant tissues: a review. *Front Plant Sci*. 2016;7:1-16. https://doi.org/10.3389/fpls.2016.00060.